

Response Surface Methodology for Development and Optimization of Theophylline Pulmonary Delivery System

Ali A. Yas^{*1}, Yehia I. Khalil^{*} and Mohamed S. Mohamed^{**}

^{*}Department of Pharmaceutics, College of Pharmacy, University of Baghdad, Baghdad, Iraq.

^{**}Department of Pharmaceutics, Fakulti Farmasi, Universiti Teknologi Mara, Selangor, Malaysia.

Abstract

The aim of the present study was to develop theophylline (TP) inhalable sustained delivery system by preparing solid lipid microparticles using glyceryl behenate (GB) and poloxamer 188 (PX) as a lipid carrier and a surfactant respectively. The method involves loading TP nanoparticles into the lipid using high shear homogenization – ultrasonication technique followed by lyophilization. The compositional variations and interactions were evaluated using response surface methodology, a Box – Behnken design of experiment (DOE). The DOE constructed using TP (X_1), GB (X_2) and PX (X_3) levels as independent factors. Responses measured were the entrapment efficiency (% EE) (Y_1), mass median aerodynamic diameter (MMAD, μm) (Y_2), zeta potential (ZP, ξ) (Y_3), fine particles fraction (% FPF) (Y_4) and percentage of dissolution efficiency at 420 minutes (% DE₄₂₀) (Y_5). The optimized formula was characterized by differential scanning calorimetry (DSC), Fourier transform infrared spectroscopy (FTIR), scanning electron microscopy (SEM) and X – ray powder diffraction (XRD) demonstrated that prolonged release physically due to the loaded TP exists mostly in its crystalline state. Analysis of dissolution data of the optimized formula indicated that the best fitting is with Higuchi model, whereas the mechanism of drug release pattern follows anomalous or non – Fickian diffusion.

Key words: Glyceryl behenate, solid lipid microparticles, theophylline nanoparticles

منهج الرد السطحي لتطوير نظام تحرير رئوي للثيوفيلين

علي احمد ياس^{*1}، يحيى اسماعيل خليل^{*} و محمد سلامة محمد^{**}

^{*} فرع الصيدلانيات، كلية الصيدلة، جامعة بغداد، بغداد، العراق .
^{**} فرع الصيدلانيات، كلية الصيدلة، الجامعة التكنولوجية مارا، سيلانكور، ماليزيا .

الخلاصة

الهدف من الدراسة هو تحضير صيغة دوائية بطيئة التحرر من الثيوفيلين بشكل جسيمات دهنية مجهرية معدة للاستنشاق باستخدام غليسيريل بهينيت كناقل دهني و البولوكسامير 188 كمثبت سطحي. طريقة التحضير تتضمن تحميل الجسيمات النانوية للثيوفيلين في الناقل الدهني باستخدام تقنية معدلة تشمل تجانس عالي ال شدة – امواج فوق صوتية يليها تخفيف بالتجميد . تقييم التغيرات التركيبية و التفاعلية باستخدام الاستجابة المنهجية السطحية , تصميم بوكس – بينكين التجريبي. التصميم التجريبي تم تشييده باعتماد عوامل مستقلة و هي الثيوفيلين (X_1), غليسيريل بهينيت (X_2) و البولوكسامير 188 (X_3) و ردود قياسية و هي كفاءة الانحباس (Y_1), متوسط القطر الايرودايناميكي (Y_2), الزيتا الاحتمالية (Y_3), نسبة الجسيمات الدقيقة (Y_4) و نسبة الكفاءة المنوية للانحلال (Y_5). ثبت للصيغة المثالية بعد اجراء المسح التفاضلي الحراري. تحويل فورييه للطيفي للاشعة تحت الحمراء, المسح المجهرى الالكتروني و حيود الاشعة السينية للمسحوق ان التحرر الطويل الامد سببه ان معظم الثيوفيلين المحمل موجود بصيغة بلورية و ان التحرر يتبع نموذج هيجوتشي و لكن الية التحرر تتبع غير فيكيان.

الكلمات المفتاحية: غليسيريل بهينيت ، الدهون الصلبة المجهرية ، جسيمات الثيوفيلين النانوية .

Introduction

Pulmonary drug delivery in comparison to other routes of administration is most promising for local respiratory diseases (e.g., asthma, chronic obstructive pulmonary disease, tuberculosis, cystic fibrosis and cancer) as well as systemic diseases (e.g., thrombosis and diabetes)⁽¹⁾. Drug targeting via inhalation result

a rapid drug deposition in a higher concentration at the site of action within lung tissues, thereby reducing the dose required and the side effects⁽²⁾.

Dry powder inhalers (DPI_s) are more preferable for delivering dry particulate drug to the respiratory tract, since they do not contain propellants as in the pressurized metered – dose

¹Corresponding author E-mail: alistein76@yahoo.com

Received: 13/10/2012

Accepted: 16/3/2013

inhalers (pMDI_s), ensure drug stability and better patient compliance due to breath – actuated⁽³⁾. For an efficient conducting airways deposition, the particle size should be in the range of 2.5 – 6 μm, suitable shape, density and surface chemistry^(4, 5). Sustained delivery inhalation therapy prolongs the duration of action and hence reduces dosing frequency⁽⁶⁾. Although liposomes – based systems are biocompatible and tolerable, they are costly to be prepared and unstable during storage and nebulization⁽⁷⁾. Polymeric nano – and micro – particles incorporated drug are prone to pulmonary toxicity, inefficient biodegradation, polymer accumulation and requirement of organic solvents for their production⁽⁸⁾. Solid lipid microparticles which are solid lipid cores stabilized by surfactants; represent a unique sustained release inhalation therapy, prepared from biocompatible and biodegradable natural lipids with good tolerability and less respiratory toxicity⁽⁹⁾. Nocturnal asthma is when asthma symptoms show exacerbation in the early hours of the morning and is associated with increased morbidity and lowered quality of life⁽¹⁰⁾. Uniphyll[®] 400 – 600 mg extended release tablets of TP, produced using CONTIN[®] chronopharmaceutical technology and administered once daily at evening for treating nocturnal asthma⁽¹¹⁾. The inter – individual variability of TP absorption especially during night and the ubiquitous of cyclic nucleotide phosphodiesterases (PDE_s) enzymes that TP non – selectively inhibit results in a wide systemic side effects, necessitate pulmonary targeting preparation^(12, 13). According to the biopharmaceutics classification system (BCS); TP is a Class I drug and in order to enhance loading and prolong its release from lipid microparticles, TP nanoparticles were prepared^(14, 15). This research focuses on the preparation, optimization and characterization of TP inhalable solid lipid microparticles.

Materials and Methods

Materials

Pure theophylline (TP) and stearic acid (SA) were purchased from (Sigma – Aldrich / USA). Glycerol behenate (GB) (Compritrol[®] 888 ATO) was a gift from (Gattefosse / France). Poloxamer 188 (PX) (Lutrol[®] F 68) was purchased from (BASF – Ludwigshafen / Germany). All other chemicals / solvents used were of analytical grade.

Methods

Design of experiment

Box – Behnken Design is a class of second – order designs based on three – level incomplete factorial designs⁽¹⁶⁾. A design of three parts, each of two fully – leveled factors and a third factor set at zero level. The dots on the surface of a sphere are lying at on the middle of each edge of multidimensional cube and center point replicate (n = 3) was designed using (Design – Expert[®] Software Version 8.0.7.1 / USA). This model is described by the following quadratic equation:

$$Y = T_0 + T_1X_1 + T_2X_2 + T_3X_3 + T_{12}X_1X_2 + T_{13}X_1X_3 + T_{23}X_2X_3 + T_{11}X_1^2 + T_{22}X_2^2 + T_{33}X_3^2 \quad (\text{Eq. 1})$$

where Y is the measured response associated with each factor level combinations; T₀ is the intercept and T₁ to T₃₃ are the regression coefficient computed from the observed value of Y; X₁, X₂ and X₃ are coded level of independent variables. The X_iX_j (i = 1, 2 or 3 and j = 1, 2 or 3) and X_i² (i = 1, 2 or 3) are interaction and quadratic terms, respectively. The independent factors selected were TP (X₁), GB (X₂) and PX (X₃). The dependent responses studied were the % EE (Y₁), MMAD, d_{aer} (Y₂), ZP, ξ (Y₃), % FPF (Y₄) and % DE₄₂₀ (Y₅). Box – Behnken design exhibit important advantages in comparison with other experimental designs: three factors are needed, and only twelve runs plus three replicates at the center point are required, costing less time and energy, each factor is studied and coded at three basic levels and it does not concern factors at extremely high or extremely low levels to avoid experiments in extreme conditions under which undesirable results might occur⁽¹⁷⁾. The composition of the Box – Behnken experimental design / factors levels are shown in (table 1).

Preparation of theophylline nanoparticles

Theophylline 250 mg and stearic acid 75 mg were dissolved in a mixture of dimethylformamide: ethanol, 45: 5 ml and then allowed to mix overnight. The solution was added to a beaker contained distilled water 50 ml via a microsyringe under sonication using a probe sonicator (Vibra – CellTM / USA) at 35% amplitude – 20 second cycles for 6 minutes. The resulting nanosuspension was stored at – 80 °C freezer (GFL[®] / Germany) and then lyophilized using a freeze dryer (Labconco[®] / USA). Directly after nanosuspension preparation, sample of 2 ml was added to the quartz cell of the photon correlation spectroscopy (Malvern

Zetasizer 1600 / UK) for zeta potential, mean particle size diameter and polydispersity index measurements. After lyophilization, the recovery was calculated using the following equation:

$$\text{Recovery} = \frac{W_p}{W_i} \times 100 \quad (\text{Eq. 2})$$

where W_p – produced solid powder weight after lyophilization, W_i – initial powder weight added of both TP and SA⁽¹⁸⁾.

Preparation of theophylline solid lipid microparticles

The process parameters were optimized for the preparation of microparticles. Theophylline nanoparticles (TP – NPs) weight equivalent to TP (0.025, 0.050 or 0.100 gm) was added to a beaker containing molten GB (1.25, 2.50 or 5.00 gm) on a hot plate (Favorit / Malaysia) at 10 °C above GB melting point. The mixture was then subjected to high shear homogenization using (X 120 CAT / Germany) at 15000 rpm for 3 minutes to allow dissolution / dispersion of TP. The still molten mass was then rapidly cooled at – 20 °C freezer (Hitachi / Japan) for 2 days. The solidified mass was thoroughly grounded in a mortar and the obtained microparticles were dispersed in a 4 °C – 25 ml aqueous phase of (1, 2 or 3 % w / v) PX, homogenized at 15000 rpm

for another 3 minutes and finally sonicated at 70 % amplitude – 20 second cycles for 12 minutes for cavitation forces to aid in further size reduction. The obtained suspension was stored at – 80 °C freezer and then lyophilized to obtain water free microparticles⁽¹⁹⁾.

Entrapment / Loading efficiency (% EE – Y₁)

Solid lipid microparticles weight approximately equivalent to TP 2 mg from each formula was washed on a filter with distilled water to remove the uncoated drug particles. Then the washed microparticles were added to 100 ml of distilled water heated up to 10 °C above excipients melting point on a hotplate magnetic stirrer using (Daihan Hotplate Stirrer / Korea) and then stir at 1500 rpm for 5 minutes to extract TP. After being cooled to room temperature, the extract is filtered through 0.45 µm syringe filter and the content was determined spectrophotometrically at 274 nm against filtered extract from TP free solid lipid microparticles as a blank using spectrophotometer (Hitachi / Japan). The entrapment efficiency (EE) and the loading efficiency (LE) were calculated by the following equations:

Table 1: Box–behnken experimental design/factors/levels

Formulation	TP (gm, X ₁)	GB (gm, X ₂)	PX (% w / v, X ₃)
F1	+1	0	+1
F2	-1	0	+1
F3	+1	0	-1
F4	0	+1	-1
F5	-1	+1	0
F6	+1	+1	0
F7	0	0	0
F8	0	+1	+1
F9	0	-1	-1
F10	+1	-1	0
F11	-1	0	-1
F12	0	0	0
F13	0	0	0
F14	-1	-1	0
F15	0	-1	+1
Factor	Level (-)	Level (0)	Level (+)
X ₁	0.025	0.050	0.100
X ₂	1.25	2.50	5.00
X ₃	1	2	3

$$EE = \frac{W_f}{W_i} \times 100 \quad (\text{Eq. 3})$$

where W_f – TP weight in the finished microparticles and W_i – TP weight initially added in the formulation.

$$LE = \frac{W_{TP}}{W_M} \times 100 \quad (\text{Eq. 4})$$

where W_{TP} – TP weight in the microparticles and W_M – microparticles weight⁽²⁰⁾.

Mass Median Aerodynamic Diameter (MMAD, $d_{aer} - Y_2$)

The solid lipid microparticles mass median aerodynamic diameter (MMAD, d_{aer}) for

each prepared formula was calculated by the following equation:

$$d_{\text{aer}} = d \times \sqrt{\frac{\rho}{\rho_1}} \quad (\text{Eq. 5})$$

where d_{aer} – aerodynamic diameter, d – mass mean geometric diameter, ρ – particles density and ρ_1 – reference density ($1 \text{ gm} / \text{cm}^3$)⁽²¹⁾. The mean mass geometric diameter (d_{50}) for each formula was measured by diluting a certain amount of solid lipid microparticles with distilled water, sonicated for 1 minute and then added to the sample dispersion unit of the laser diffractometer (Malvern Mastersizer 2000 / UK)⁽²²⁾. The particles density (ρ) measurement was done by placing a certain amount of microparticles in a graduated cylinder, heated up to 10°C above excipients melting point and after being cooled to room temperature the final volume measured, according to the following equation:

$$\rho = \frac{m}{v} \quad (\text{Eq. 6})$$

where ρ – density of the solid lipid microparticles, m – weight of the solid lipid microparticles and v – volume of the molten lipid microparticles at room temperature⁽²³⁾.

Zeta potential (ZP, $\zeta - Y_3$)

After samples being diluted with distilled water and sonicated for 1 minute, the zeta (ζ) – potential is determined automatically by the photon correlation spectroscopy, by placing the solid lipid microparticles suspension in an electric field and measuring their mobility which is then related to the ζ at the interface, using the Smoluchowski equation:

$$\zeta = \frac{U_E \eta}{\varepsilon} \quad (\text{Eq. 7})$$

where ζ – zeta potential (mV), U_E – electrophoretic mobility (cm / sec), η – medium viscosity (centipoise) and ε – dielectric constant⁽²⁴⁾.

Fine particles fraction (% FPF – Y_4)

In order to evaluate the in vitro aerosolization efficiency of the solid lipid microparticles; Andersen Cascade Impactor (ACI) (Graseby / USA) was used. The cascade impactor consists of a throat, a preseparator and eight stages of impaction plates (0 – 7) with cutoff aerodynamic diameters of 9, 5.8, 4.7, 3.3, 2.1, 1.1, 0.65 and $0.43 \mu\text{m}$ respectively. The impaction plates were precoated with a 2 % w / v of hydroxypropylmethylcellulose (4000 cps) gel in water to prevent particles bouncy and re – entrainment. A size “2” hard gelatin capsules were filled with 20 mg powder from each prepared sample and aerosolized using

Rotahaler[®] (Cipla / India). The inhalation test was performed at an inhalation rate of $28.3 \text{ L} / \text{minute}$ for 10 seconds. The fine particles fraction, which is total percentage deposited at stage 2 – 7 of the cascade impactor was used to evaluate aerosol performance using the following equation:

$$\text{FPF} = \frac{\text{FPD}}{\text{TD}} \times 100 \quad (\text{Eq. 8})$$

where FPF – fine particles fraction, FPD – fine particles dose (i.e., total weight of the solid lipid microparticles with size $\leq 5 \mu\text{m}$) and TD – total dose weight of the solid lipid microparticles delivered from the mouthpiece of the inhaler into the apparatus⁽²⁵⁾.

Dissolution efficiency (% $DE_{420} - Y_5$)

The in vitro release was performed using Franz diffusion cell system (PermeGear / USA). The receiver compartment was filled with 21 ml phosphate buffer pH 7.4, maintained at $37 \pm 0.5^\circ \text{C}$ and stirred magnetically at 100 rpm. A cellulose acetate membrane ($0.45 \mu\text{m}$ pore size and 2.5 cm^2 surface area) was inserted between the donor and the receptor compartments. A suitable aliquot of the solid lipid microparticles equivalent to TP 0.4 mg from each prepared sample was evenly spread on the cellulose acetate membrane that is pre – moistened with phosphate buffer pH 7.4 containing 0.1 % w / v Tween 80 as a wetting agent and was occluded with a paraffin film. At time intervals of (5, 10, 15, 30, 60, 120, 180, 240, 300, 360 and 420 minutes), 3 ml aliquots of the receptor fluid were withdrawn, replaced by an equal volume of fresh medium and assayed spectrophotometrically against phosphate buffer pH 7.4 as a blank⁽²⁶⁾. Relying on correction for sampling, TP cumulated amount released Q was calculated using the following equation:

$$Q = V_s \times \sum_{n=1}^n c_n - 1 + V_m \times C_n \quad (\text{Eq. 9})$$

where V_s – volume of sample withdrawn, C_{n-1} – drug concentration of the sample and V_m – volume of the receptor medium⁽²⁷⁾. The magnitude percentage of dissolution efficiency at 420 minutes (% DE_{420}) for each prepared sample was calculated from the area under the curve at time t and measured using the trapezoidal rule and expressed as a percentage of the area of the rectangle described by 100 % dissolution in the same time using the following equation⁽²⁸⁾:

$$\% DE_{420} = \left(\frac{\int_0^t \frac{y \times dt}{100 \times t} \right) \times 100 \quad (\text{Eq. 10})$$

The release data of TP formulas was fitted into various release kinetic models⁽²⁹⁾ (Table 2).

Table 2: Mathematical models and dissolution mechanisms describing release kinetics.

Model	Mechanism	Equation
Zero – Order	Concentration Independent	% r = $K_0 t$ (Eq. 11)
First – Order	Concentration Dependent	% r = $100 (1 - e^{-K_1 t})$ (Eq. 12)
Higuchi	Diffusion	% r = $K_H t^{0.5}$ (Eq. 13)
Hixson – Crowell	Erosion	% r = $100 (1 - (1 - \frac{KHC t}{4.6416}))$ (Eq. 14)
Korsmeyer – Peppas	Diffusion	% r = $K_{KP} t^n$ (Eq. 15)

Where % r – cumulative % TP released at time t, K – rate constant of the model and n – release exponent

Checkpoint analysis

The checkpoint analysis was performed to confirm the reliability of the equations and plots in responses prediction. Independent variables values were taken at three points / levels (0, -0.5, 0.5), (0.5, 0, -0.5) and (-0.5, 0.5, 0). Solid lipid microparticles formulations at these three checkpoints were prepared experimentally as shown in (Table 3) and evaluated for the responses by analyses in triplicate to ensure reproducibility⁽³⁰⁾.

Table 3: Checkpoint formulas

Formulas	X ₁	X ₂	X ₃
F16	0	-0.5	0.5
F17	0.5	0	-0.5
F18	-0.5	0.5	0

Optimization of the Solid Lipid Microparticles Preparations

In order to get the optimized formula (F₀), the desirability function was run using Design – Expert[®] Version 8.0.7.1 Software. The optimum formula was based on list criteria of maximum entrapment / loading efficiency, mass median aerodynamic diameter (MMAD ≤ 5 μm), zeta potential (≥ ± 30 mV), maximum fine particles fraction and maximum cumulative percentage release in 420 minutes.

Differential scanning calorimetry

Thermal analyses were performed using differential scanning calorimeter (DSC – Perkin Elmer / USA). Under nitrogen flow of 20 ml / minute, approximately 2 mg of pure TP, GB, SA, TP – NPs, TP – GB physical mixture (1: 3) and F₀ was placed in a crimp – sealed aluminum pan and heated from 10 – 300 °C at a scanning rate of 10 °C / minute. An empty aluminum pan was used as a reference.

Fourier transform infrared spectroscopy

Fourier transform infrared spectroscopy was performed using (FTIR – Perkin Elmer /

USA) in order to characterize the possible interactions between the drug and the carrier in the solid state. Samples of pure TP, GB, SA, TP – NPs, TP – GB physical mixture and F₀ were prepared according to the KBr disc method. The scanning range was 4000 – 450 cm⁻¹ and the resolution was 4 cm⁻¹.

Scanning electron microscopy

The scanning electron microscopy analyses were performed using (FESEM – FEI / Netherland). Samples of pure TP, TP – NPs and F₀ were mounted onto aluminum stubs and coated with a thin platinum layer. The scanning electron microscope was operated at an acceleration voltage of 5 KV and working distance of 7 – 10 mm.

X – ray powder diffraction

The powder X – ray diffraction patterns were recorded using (Rigaku XRD / Japan), under the following conditions: target CuK_α monochromatized radiation, voltage 40 KV and current of 20 mA at ambient temperature. The data of pure TP, GB, SA, TP – NPs, TP – GB physical mixture and F₀ were collected in the continuous scan mode from 2° – 40° (2θ) at an angular increment of 0.02° / second and count time of 1second / step.

Results and Discussions

Theophylline nanoparticles characterization

Stearic acid was chosen as a stabilizer because it is naturally found in a small amount in the surfactant layer lying the lung epithelium, solid at room temperature and an amphiphilic surfactant that will act as an interface between TP – NPs and water phase⁽³¹⁾. The TP – NPs characterizations are shown in (Table 4) and (Figure 1).

Table 4: Theophylline nanoparticles racterizations

ζ (mV)	d ₅₀ (nm)	PI	%Recovery
- 41.205 ±1.453	722.040 ±6.677	0.558 ±0.031	75.361 ±16

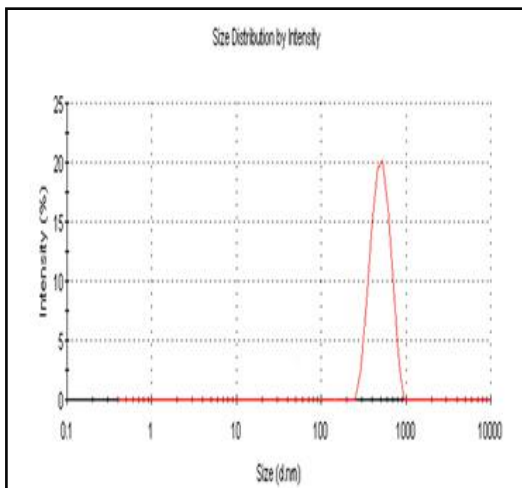


Figure 1: TP – NPs Size distribution – size statistics report by intensity

Theophylline solid lipid microparticles preparation

The rapid cooling leads to formation of solid solution (homogenous distribution) of drug in lipid matrix. Drug release takes place by diffusion from the matrix and upon lipid degradation in vivo (Figure 2) (32).

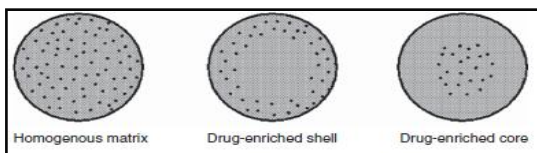


Figure 2: Three incorporation models of drugs in the solid lipid matrix

Entrapment / Loading efficiency (% EE – Y₁)

The entrapment efficiency (EE) varies from 34.762 % (F14) to 95.989 % (F3) for various factors level combinations (Table 5). The independent factors affecting the EE were TP (X₁) and PX (X₃) levels (P < 0.05, Tables 6 – 7) and (Figure 3). TP has a significant – positive effect on the EE. Although TP hydrophilicity

favors the external aqueous phase, its EE_s in some formulations were high, because TP localized at the interface (i.e., solid lipid microparticles surfaces) will induce outer surface saturation at higher concentrations and besides the internal phase viscosity (i.e., GB solidity due to its high melting point) will reduce TP leakage by reducing the external aqueous phase entrance into the lipid matrix (33, 34).

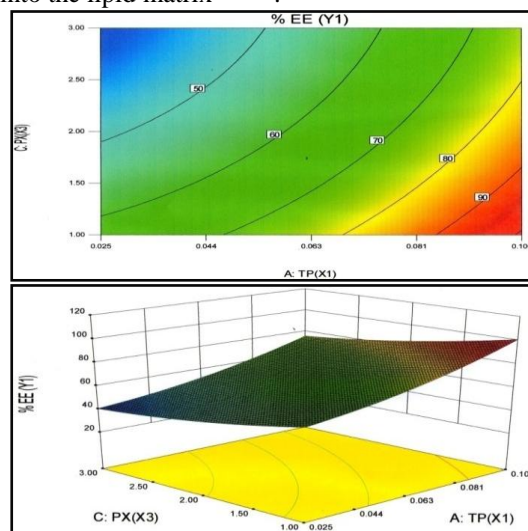


Figure 3: Response surface contour plot (Up) and 3D plot (down) for TP and PX effect on EE.

Table 5: Observed responses

Formulation	% EE (Y ₁)	MMAD d _{aer} μm (Y ₂)	ZP ξ mV (Y ₃)	% FPF ≤ 5 μm (Y ₄)	% DE ₄₂₀ (Y ₅)
F1	75.964±5.463	4.849±0.456	-34.366±1.187	36.792±1.055	73.782±5.533
F2	47.596±6.458	4.902±0.227	-26.850±1.282	35.816±1.773	44.156±3.109
F3	95.989±4.146	6.168±0.083	-32.066±0.375	24.725±0.800	75.189±6.496
F4	67.017±7.147	6.514±0.149	-23.566±0.301	23.742±1.606	50.547±4.601
F5	51.578±4.542	6.104±0.229	-22.450±1.837	34.598±0.888	47.786±2.512
F6	85.263±3.917	6.225±0.196	-31.316±0.957	33.808±0.862	76.210±4.414
F7	56.428±5.931	6.232±0.209	-27.300±0.312	32.466±0.781	52.135±3.791
F8	41.578±3.605	5.278±0.478	-25.433±0.301	38.736±0.885	38.629±1.254
F9	78.247±5.174	6.456±0.106	-28.216±0.028	24.674±0.596	70.089±4.460
F10	83.789±6.955	6.099±0.064	-30.683±0.161	35.878±0.962	77.708±6.095
F11	58.754±5.777	6.354±0.205	-27.733±0.189	22.677±0.808	46.812±3.213
F12	55.357±5.896	6.181±0.208	-28.166±0.602	32.343±0.503	51.971±4.218
F13	55.714±5.786	6.283±0.211	-27.983±0.425	32.905±0.639	51.553±3.989
F14	34.762±4.301	6.256±0.213	-20.200±0.100	34.615±1.356	42.878±2.214
F15	39.368±3.568	5.115±0.224	-25.916±1.537	37.703±1.114	47.799±2.121

Table 6: Statistical regression analysis

Parameters	% EE (Y ₁)		MMAD d _{aer} μm (Y ₂)		ZP ξ mV (Y ₃)		% FPF ≤ 5 μm (Y ₄)		% DE ₄₂₀ (Y ₅)	
	Coefficient	P-Value	Coefficient	P-Value	Coefficient	P-Value	Coefficient	P-Value	Coefficient	P-Value
Intercept	62.220	0.0241	6.240	<0.0001	-29.380	0.0309	32.370	<0.0001	55.230	0.0453
X ₁ (0.025, 0.100)	18.240	0.0019	-0.024	0.3918	-3.940	0.0019	0.330	0.1202	15.150	0.0023
X ₂ (1.25, 5.00)	0.860	0.7907	0.035	0.2393	0.240	0.7247	-0.350	0.1007	-3.170	0.2847
X ₃ (1.00, 3.00)	-11.750	0.0138	-0.660	<0.0001	-0.430	0.5534	6.690	<0.0001	-4.300	0.1750
X ₁ x X ₂	-1.790	0.6758	0.061	0.1319	-0.220	0.8101	-0.640	0.0395	-0.040	0.9913
X ₁ x X ₃	-0.700	0.8731	0.026	0.4944	-0.880	0.3666	-0.340	0.2168	1.560	0.6801
X ₂ x X ₃	1.840	0.6753	0.034	0.3748	-0.960	0.3271	0.560	0.0653	1.350	0.7204
X ₁ x X ₁	4.880	0.3820	-0.170	0.0096	-0.120	0.9151	0.370	0.2663	4.150	0.3876
X ₂ x X ₂	-3.250	0.5514	0.110	0.0504	3.340	0.0279	1.990	0.0011	1.770	0.7029
X ₃ x X ₃	3.120	0.5115	-0.490	<0.0001	-1.040	0.3209	-3.080	<0.0001	-0.640	0.8725
R ²	0.9244		0.9946		0.9158		0.9971		0.9002	

Table 7: Analysis of variance (ANOVA)

Response	Source	Degree of Freedom	Sum of Square	Mean of Square	Fischer's Ratio (F)	Probability > F*	Standard Deviation	Coefficient of Variance (%)
% EE (Y ₁)	Model	9	4407.100	489.680	6.800	0.0241	8.490	13.730
	Error	5	360.250	72.050	-	-	-	-
	Cumulative Total	14	4767.350	-	-	-	-	-
MMAD d _{aer} μm (Y ₂)	Model	9	4.670	0.520	101.960	< 0.0001	0.071	1.200
	Error	5	0.025	0.005	-	-	-	-
	Cumulative Total	14	4.695	-	-	-	-	-
ZP ξ mV (Y ₃)	Model	9	178.980	19.890	6.040	0.0309	1.810	6.600
	Error	5	16.460	3.290	-	-	-	-
	Cumulative Total	14	195.440	-	-	-	-	-
% FPF ≤ 5 μm (Y ₄)	Model	9	408.850	45.430	191.170	< 0.0001	0.490	1.520
	Error	5	1.190	0.240	-	-	-	-
	Cumulative Total	14	410.040	-	-	-	-	-
% DE ₄₂₀ (Y ₅)	Model	9	2406.390	267.380	5.010	0.0453	7.300	12.930
	Error	5	266.750	53.350	-	-	-	-
	Cumulative Total	14	2673.150	-	-	-	-	-

*Probability > F is the significance level and a value < 0.05 considered significant

PX has a significant – negative effect on the EE. TP becomes partly negatively charged at pH < 9 (i.e., neutral pH) and this result in the absence of attractive electrostatic interactions with PX polyethylene oxide chains. In addition TP characteristic of pH independent solubility will precludes its hydrophobic interactions with the PX hydrophobic cores and the PX swelling upon hydration, all result in TP within the PX layer release increment⁽³⁵⁾. The effects on Y₁ can be explained by the following quadratic equation:

$$Y_1 = 62.22 + 18.24X_1 + 0.86X_2 - 11.75X_3 - 1.79X_1X_2 - 0.7X_1X_3 + 1.84X_2X_3 + 4.88X_1^2 - 3.25X_2^2 + 3.12X_3^2$$

(Eq. 16)

There is an inverse relationship between the aqueous surfactant concentration and the sonication time but to a certain limit, because less energy will be required to achieve maximum dispersion of the produced solid lipid microparticles. Any increase in PX concentration will not aid in coverage, in contrary will lead to an increment in the micelles formation which has more negative effect on TP – solid lipid microparticles EE⁽³⁶⁾.

Mass median aerodynamic diameter (MMAD, d_{aer} – Y₂)

The aerodynamic diameter is the diameter of a sphere of unit density, which reaches the same velocity in the air stream as a non – spherical particle of arbitrary density and expresses the mechanism of particle deposition in the

respiratory system ⁽³⁷⁾. The mass median aerodynamic diameter [MMAD, d_{aer}] ranged from 4.849 μm (F1) to 6.514 μm (F4) (Table 5) with the selected levels of variables. The most factors affecting the MMAD are PX (X_3 and X_3^2) and TP (X_1^2) ($P < 0.05$, Tables 6 – 7) and (Figures 4 - 5). PX has a significant – negative effect on the MMAD.

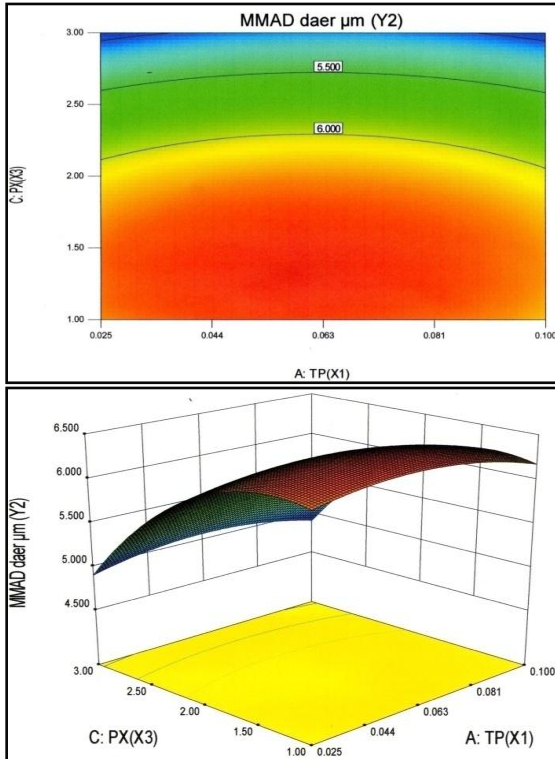


Figure 4: Response surface contour plot (Up) and 3D plot (down) for TP and PX effect on MMAD

Generally, independent on the PX molecular weight, the preserving of the MMAD values is due to the PX efficient coverage of the surfaces and sterically stabilizing microparticles by its long hydrophilic polyethylene oxide chains (poloxamer 188 average number of ethylene oxide ≈ 153 units) extend into solution and shield the particles surfaces preventing their agglomeration during the homogenization and sonication processes. Also, these hydrophilic arms will potentially influence the shape of the resulting particles ⁽³⁸⁾. TP has a significant – negative effect on the MMAD. This is attributed to the concentration effect of the non – incorporated TP molecules during lyophilization results in the formation of highly concentrated solutions of TP that its ionization will affect the ZP and particles agglomeration. ⁽³⁹⁾. Y_2 can be described by the following quadratic equation:

$$Y_2 = 6.24 - 0.024X_1 + 0.035X_2 - 0.66X_3 + 0.061X_1X_2 + 0.026X_1X_3 + 0.034X_2X_3 - 0.17X_1^2 + 0.11X_2^2 - 0.49X_3^2 \quad (\text{Eq. 17})$$

A part of the PX covering layer of the solid lipid microparticles surfaces removed, a reduction in the repel force impart by PX steric hindrance, enhance particles agglomeration through Van der Waals forces of attraction between particles and hence there will be an increase in the mean solid lipid microparticles size after freeze drying process ⁽⁴⁰⁾.

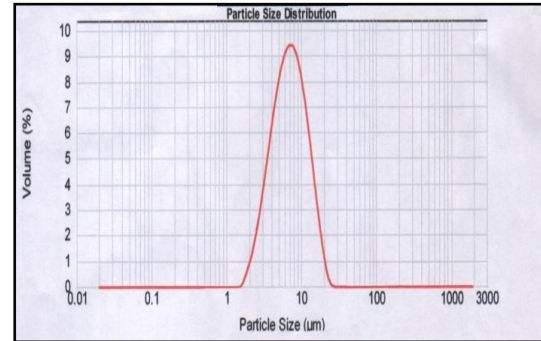


Figure 5: Particle size distribution of the F₀

Zeta potential (ZP, $\zeta - Y_3$)

The zeta (ζ) – potential (ZP) is the electrostatic potential at the boundary dividing the compact layer (charged solid surface – immobile counterions) and the diffuse layer (liquid counterions – mobile counterions) ⁽⁴¹⁾. The ZP (> 30 or < -30 mV), indicates electrostatic repulsion among particles and good stability ⁽⁴²⁾. The ZP values varied from – 34.366 mV (F1) to – 20.200 mV (F14) (Table 5). TP (X_1) and GB (X_2^2) have statistical influential effects on the ZP ($P < 0.05$, Tables 6 – 7) and (Figures 6 – 7). TP has a significant – negative effect on the ZP. This is attributed to the free not incorporated TP that will be partly negatively charged at neutral pH and the increase in the ZP will be in the negative direction ⁽⁴³⁾.

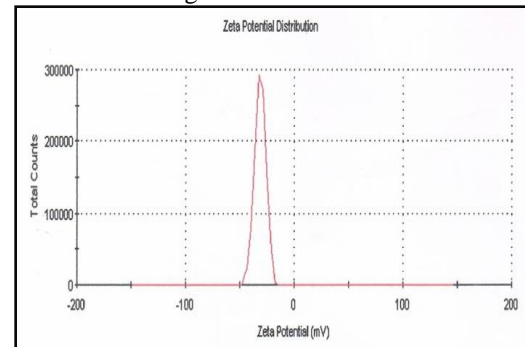


Figure 6: Zeta potential distribution of the F₀

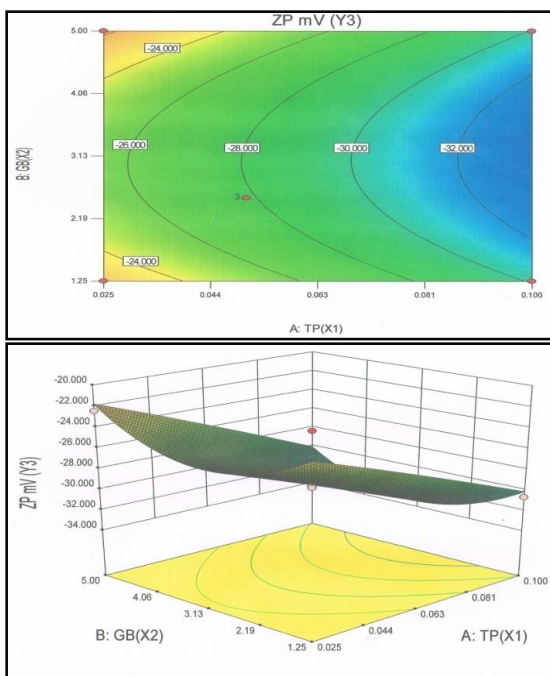


Figure 7: Response surface contour plot (Up) and 3D plot (down) for TP and GB effect on ZP

GB has a quadratic significant – positive effect on the ZP. As GB content increased, there will be a reduction in the solid lipid microparticles pH together with ZP increment in the positive direction due to the solid lipid microparticles surfaces TP protonation at low pH (pH < 4) (44). Both factors effects on Y₃ are shown in the quadratic equation below:

$$Y_3 = -29.38 - 3.94X_1 + 0.24X_2 - 0.43X_3 - 0.22X_1X_2 - 0.88X_1X_3 - 0.96X_2X_3 - 0.12X_1^2 + 3.34X_2^2 - 1.04X_3^2 \text{ (Eq. 18)}$$

The negative charge of the solid lipid microparticles core matrixes are involved in electrostatic interaction with the weakly basic TP molecules. Thus, the solid lipid microparticles surfaces negative charge is the main contributor to the negative ZP of the solid lipid microparticles (45).

The changes in the interfacial properties will have an influential effect on the ZP and hence solid lipid microparticles size. This is due to the PX layer covering the solid lipid microparticles surfaces will reduce the ZP but will provide steric stability instead if solid lipid microparticles being efficiently covered with PX (46).

Fine particles fraction (% FPF – Y₄)

Andersen Cascade Impactor (ACI) is a primary technique used for both development and testing of the inhaler products. Size determination is based on the inertial impaction

of aerosolized particles passing through decreasing nozzle apertures onto subsequent deposition stages each with a defined aerodynamic cut – off diameter (47). The fine particles fraction (FPF) is lowest at 22.677 % (F11) and highest at 38.736 % (F8) (Table 5). PX (X₃ and X₃²) and GB (X₂²) are the most factors affecting FPF (P < 0.05, Tables 6 – 7) and (Figure 8). Simply by decreasing the cohesive forces between particles a lower aggregation tendency might gain and consequently lower surface energy was necessary to increase the flowability and finally the powder FPF. Also; by reducing the particle density and tolerating an increase of the average particle size will enhance the aerosol efficiency. PX has a significant – positive effect on the FPF. PX percentage used has a special role concerning particles morphology, dispersibility and flowability. As PX concentration increased, the FPF increased up to a certain limit that beyond highly charged particles produced (48).

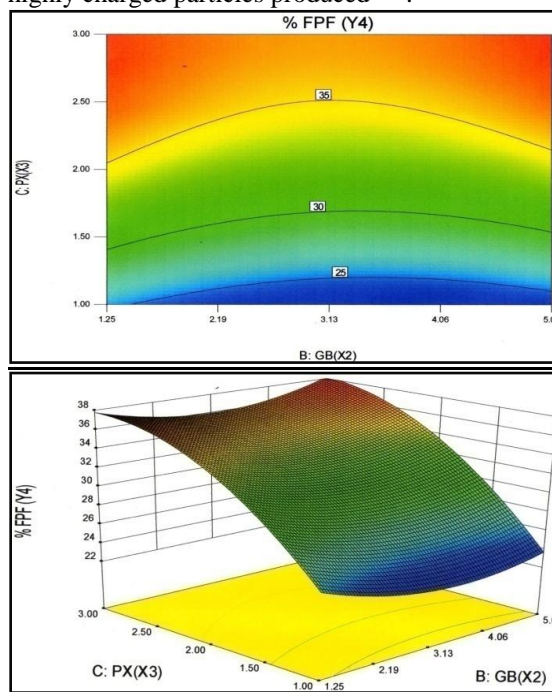


Figure 8: Response surface contour plot (Up) and 3D plot (down) for GB and PX effect on FPF

Although GB has a quadratic significant – positive effect on the FPF, but it is a slight increment and only at higher GB concentration and that is shown from the surface truncated shape of the 3D plot for the response Y₄ range. Effects of factors on response Y₄ explained by the following quadratic equation:

$$Y_4 = 32.37 + 0.33X_1 - 0.35X_2 + 6.69X_3 - 0.64X_1X_2 - 0.34X_1X_3 + 0.56X_2X_3 + 0.37X_1^2 + 1.99X_2^2 - 3.08X_3^2 \text{ (Eq. 19)}$$

GB enables the production of low density aerodynamically inhalable particles and thus improving their respirable fraction by avoiding the natural clearance mechanism of the lungs (e.g., alveolar macrophage uptake) due to the higher geometric diameter of the particles⁽⁴⁹⁾.

Dissolution efficiency (%DE₄₂₀ – Y₅)

The cumulative percentage of TP release at 420 minutes (% DE₄₂₀) varied from 38.629 % (F8) to 77.708 % (F10) (Table 5). TP (X₁) is the only factor affecting the % DE₄₂₀. TP has a significant – positive effect on the % DE₄₂₀ (P < 0.05, Tables 6 – 7) and (Figure 9). Concerning TP effect only; TP release is biphasic, the first phase was a slight burst release due to the free non – incorporated TP on the solid lipid microparticles surfaces followed by prolong release due to the incorporated stable crystalline anhydrous TP⁽⁵⁰⁾.

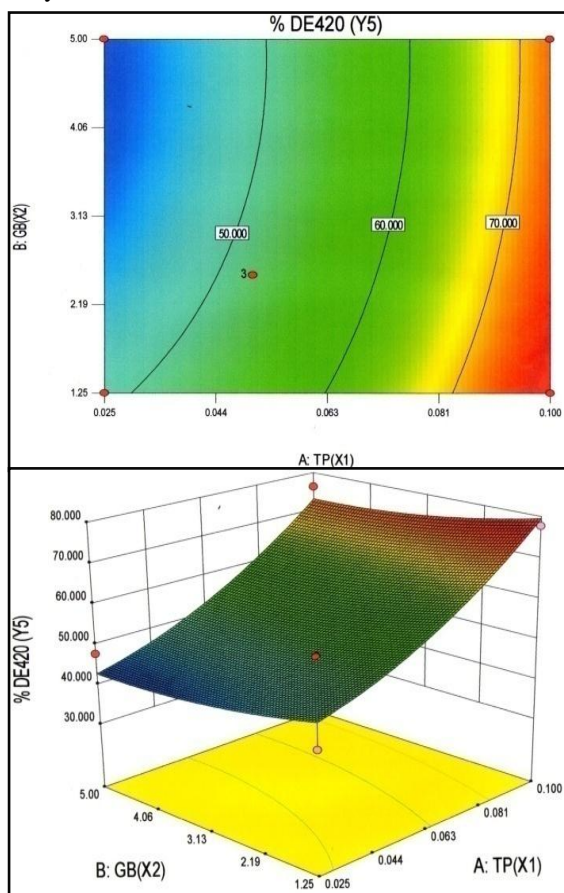


Figure 9: Response surface contour plot (Up) and 3D plot (down) for TP and GB effect on %DE₄₂₀

Concerning GB non – significant – negative effect on the % DE₄₂₀ is due to the cold homogenization technique employed in the solid lipid microparticles production which results in a solid solution drug incorporation model and GB low crystallization degree. Therefore, TP release rate will be prolonged for some formulations because the drug which is molecularly dispersed in the colloidal particles has a limited motion⁽⁵¹⁾. Percentage TP released in 420 minutes can be described by the following quadratic equation:

$$Y_5 = 55.23 + 15.15X_1 - 3.17X_2 - 4.3X_3 - 0.04X_1X_2 + 1.56X_1X_3 + 1.35X_2X_3 + 4.15X_1^2 + 1.77X_2^2 - 0.64X_3^2 \text{ (Eq. 20)}$$

The reasonable explanation for the prolonged release is the three steps govern TP release from solid lipid microparticles; entrance of the dissolution medium into the solid lipid microparticles matrixes, dissolution of the dispersed TP particles / crystals and diffusion of the dissolved TP through the inert solid lipid microparticles matrixes⁽⁵²⁾.

Checkpoint analysis

Three checkpoint formulations were prepared and evaluated for dependent responses (Table 8). Comparing the predicted and experimental values using Student t – test, the differences were found to be insignificant (p > 0.05) indicate that the obtained mathematical equation is valid for predicting the dependent responses values. (Eq. 21) was used in the percentage relative error calculation between the experimental and predicted values of each response:

$$\% \text{ Relative Error} = \frac{\text{Predicted Value} - \text{Experimental Value}}{\text{Predicted Value}} \times 100 \text{ (Eq. 21)}$$

Optimization of the solid lipid microparticles preparations

Comprehensive search through desirability function revealed that the F₀ with 0.889 desirability has the composition of 0.1 gm TP, 1.27 gm GB and 3 % w / v PX. By preparing the F₀, the experimental responses are in good agreement with the predicted values (Table 9).

Table 8: Checkpoint formulations comparing experimntal / predicted Values (n = 3)

No.	Ex.	Pr.	% RE
F16			
% EE Y ₁	60.187±3.074	56.740	0.060
MMAD d _{aer} μm Y ₂	6.025±0.435	6.634	0.091
ZP ζ mV Y ₃	-25.480±0.314	-23.399	0.088
% FPF Y ₄	28.356±0.367	32.225	0.120
%DE ₄₂₀ Y ₅	67.344±3.773	61.142	0.101
F17			
% EE Y ₁	87.434±4.933	81.055	0.078
MMAD d _{aer} μm Y ₂	7.234±0.763	6.139	0.178
ZP ζ mV Y ₃	-35.132±1.145	-30.434	0.154
% FPF Y ₄	17.315±0.310	15.727	0.100
%DE ₄₂₀ Y ₅	53.640±2.206	58.342	0.080
F18			
% EE Y ₁	54.345±2.629	45.132	0.204
MMAD d _{aer} μm Y ₂	6.431±0.173	5.985	0.074
ZP ζ mV Y ₃	-27.340±1.415	-24.156	0.131
% FPF Y ₄	29.346±0.381	32.637	0.100
%DE ₄₂₀ Y ₅	38.343±1.146	46.635	0.177

Table 9: Optimized formula experimntal / predicted values (n = 3)

F ₀	Ex.	Pr.	% RE
% EE Y ₁	76.246±3.582	71.923	0.060
MMAD d _{aer} μm Y ₂	6.035±0.463	4.890	0.234
ZP ζ mV Y ₃	-29.734±2.509	-31.580	0.058
% FPF Y ₄	35.819±1.343	38.731	0.075
%DE ₄₂₀ Y ₅	71.069±2.136	74.723	0.048

Mechanism of dissolution

The regression parameters obtained after fitting various release kinetic models to the in vitro dissolution data are listed in (Table 10). The fit for various models investigated for drug release of the F₀ can be arranged in the following descending order: Higuchi > Korsmeyer – Peppas > Zero – Order > Hixson – Crowell > First – Order. The exact mechanism of release is non Fickian or anomalous from the slope value of Korsmeyer – Peppas which is lie in the range of (0.450 < n < 0.890). The in vitro release profiles of TP, TP - NPs and F₀ are shown in (Figure 10). The low release percentage of crude TP powder is due to the

larger particle size in comparison with the TP – NPs and F₀.

Table 10: Release kinetic parameters of the F₀

Model	Slope	Intercept	R ²
Zero – Order	0.179	12.510	0.916
First – Order	0.003	0.933	0.578
Higuchi	3.982	-0.952	0.990
Hixson – Crowell	0.006	2.013	0.633
Korsmeyer – Peppas	0.687	0.187	0.966

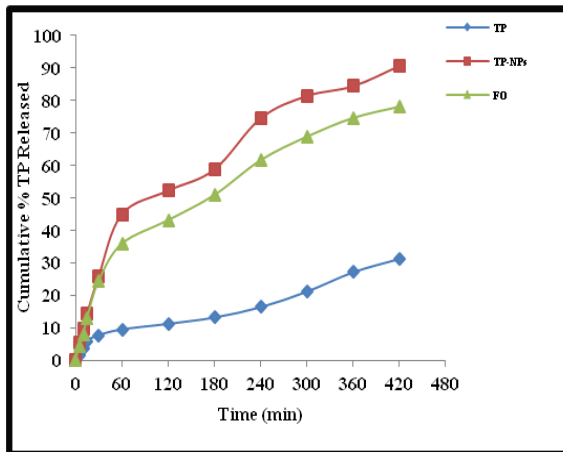


Figure 10: in vitro release profiles of TP, TP – NPs and F₀

Differential scanning calorimetry

(Figure 11) shows the DSC of pure TP, GB, SA, TP – NPs, TP – GB physical mixture and F₀ endothermic peak at 274 °C, 77.41 °C, 69.30 °C, 64.83 – 272.20 °C, 75.11 – 270.38 °C and 76.18 °C respectively. The endothermic peak corresponding to the melting point of TP is reduced to 272.20 °C in the DSC thermogram of TP – NPs and 270.38 °C in the DSC thermogram of TP – GB physical mixture respectively, and this indicated that in TP – NPs there is a lack of significant changes in TP crystalline state, whereas in the TP – GB physical mixture indicates TP saturation in the carrier. The disappearance of TP melting peak in the F₀ was noticed due to its percentage of (~ 5 % w / w) so it is lowered, broadened and becomes DSC undetectable⁽⁵³⁾.

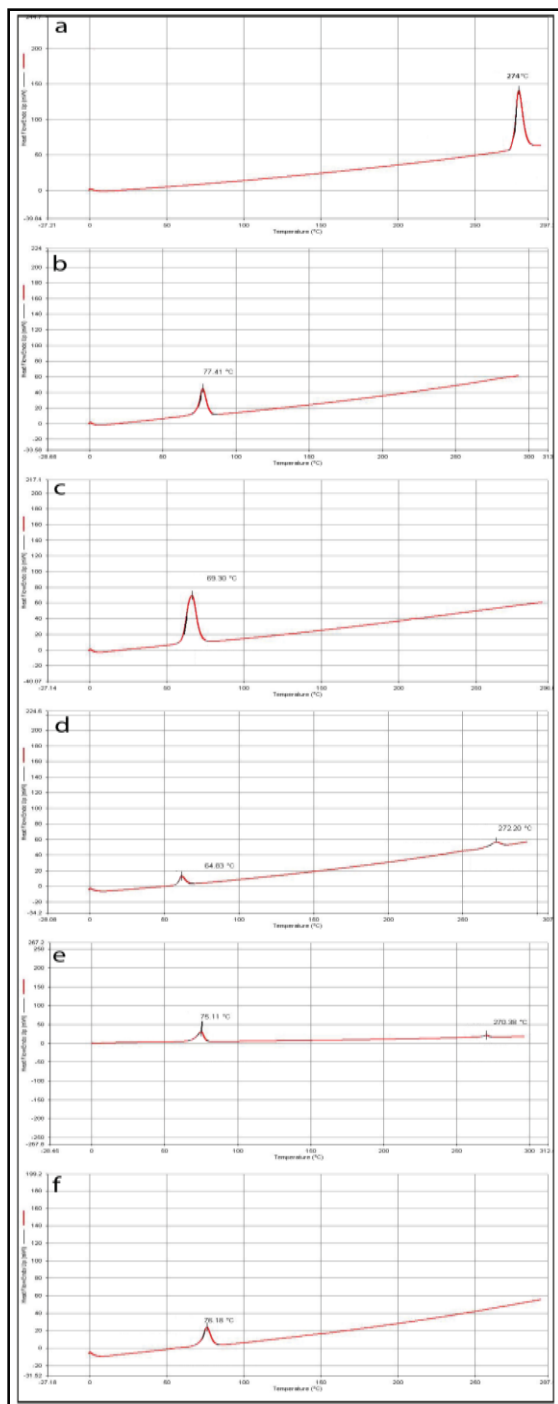


Figure 11: Differential Scanning Calorimetry Thermograms of TP (a), GB (b), SA (c), TP - NPs (d), TP - GB Physical Mixture (e) and F₀ (f)

Fourier Transform Infrared Spectroscopy

As shown in (Figure 12), the FTIR spectrum of pure TP, GB, SA, TP - NPs, TP - GB physical mixture and F₀. The spectrum of TP shows characteristic peaks at 1710 cm⁻¹ and 1665 cm⁻¹ attributable to the (C = O stretching

vibrations). The band at 1563 cm⁻¹ is attributable to the (pyrimidine ring stretching vibration)⁽⁵⁴⁾. The GB shows distinctive bands at 2916 cm⁻¹ and 2849 cm⁻¹ attributable to asymmetric and symmetric (aliphatic CH₂ stretching vibrations). The band at 1737 cm⁻¹ is attributable to the (ester C = O stretching vibration)⁽⁵⁵⁾. The spectrum of SA resembles that of GB with little shift, i.e. the asymmetric and symmetric (aliphatic CH₂ stretching vibrations) will be at 2920 cm⁻¹ and 2851 cm⁻¹ respectively, whereas the (ester C = O stretching vibration) will be at 1703 cm⁻¹. The spectrum of TP - NPs still showed the SA 2920 cm⁻¹ and 2851 cm⁻¹ bands, whereas 1703 cm⁻¹ disappear due to the TP 1710 cm⁻¹ and 1665 cm⁻¹ bands in the same region. The spectrum of TP - GB physical mixture still showed the GB bands at 2916 cm⁻¹, 2849 cm⁻¹ and 1737 cm⁻¹, whereas TP 1710 cm⁻¹, 1665 cm⁻¹ and 1563 cm⁻¹ still shown with different intensity as a consequence of TP existence on the microparticles surfaces. The spectrum of F₀ shows GB bands at 2916 cm⁻¹, 2849 cm⁻¹ and 1737 cm⁻¹, whereas TP band at 1563 cm⁻¹ is the only shown due to the TP bands at 1710 cm⁻¹ and 1665 cm⁻¹ close proximity with respect to the GB 1737 cm⁻¹ band.

Scanning electron microscopy

The scanning electron microscope images for pure TP, TP - NPs and F₀ are shown in (Figure 13). Both pure TP and TP - NPs show a prismatic TP crystal habit, whereas the F₀ image shows irregular shape particles⁽⁵⁶⁾. This irregularity is due to sonication done at 4 °C by using an ice bath to prevent lipid melting by heat generated and so drug loading and homogeneity maintained.

X - ray powder diffraction

The XRD patterns of pure TP, GB, SA, TP - NPs, TP - GB physical mixture and F₀ are shown in (Figures 14). Pure TP diffractogram has an important distinctive peak of high intensity at 12.63 ° (2θ), another two small and isolated peaks are present at 7.11 and 14.33 ° (2θ), whereas a group of small peaks covers the range 20 - 30 ° (2θ). GB has a high intensity peak at 21.22 ° (2θ) and a smaller one at 23.43 ° (2θ). SA has a high intensity peak at 2.22 ° (2θ) and two successive peaks at 21.5 ° (2θ) and 23.8 ° (2θ). TP - NPs, TP - GB physical mixture and F₀ diffractograms still showed TP, SA and GB peaks but at reduced intensity. Although TP melting peak disappearance in the F₀ corresponding DSC curve, TP isolated peaks in the above diffractograms confirms its crystalline state.

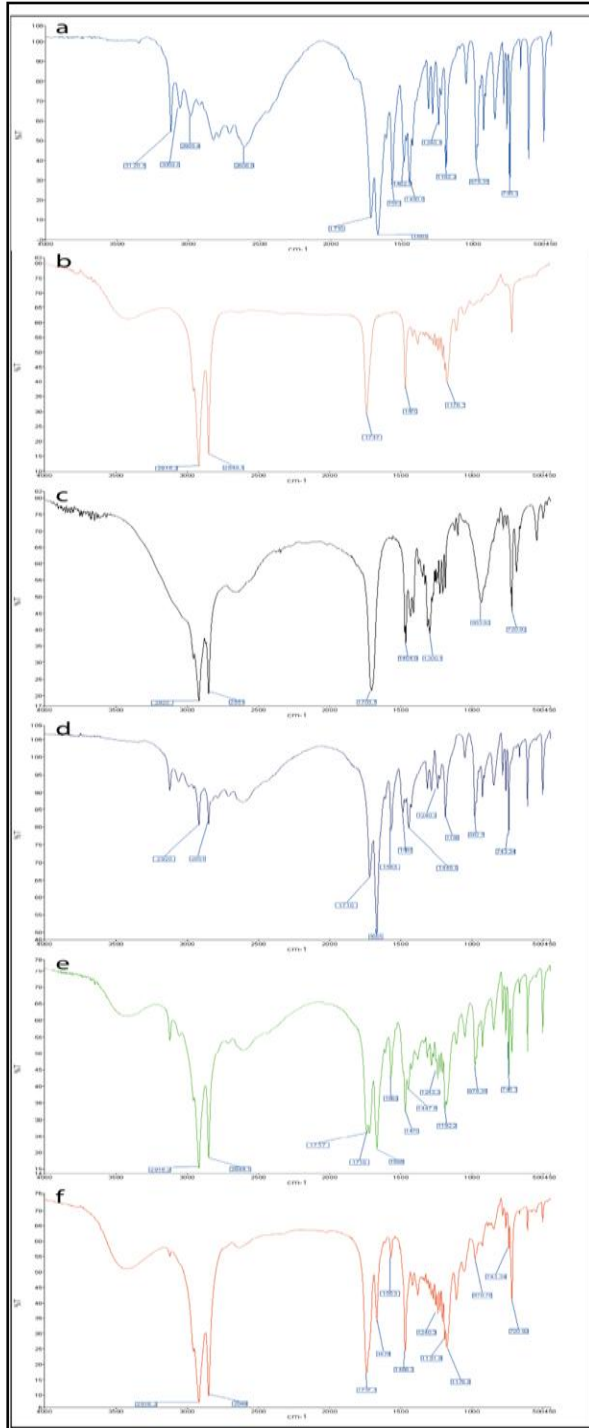


Figure 12: Fourier transform infrared images of TP (a), GB (b), SA (c), TP – NPs (d), TP – GB physical mixture (e) and F₀ (f)

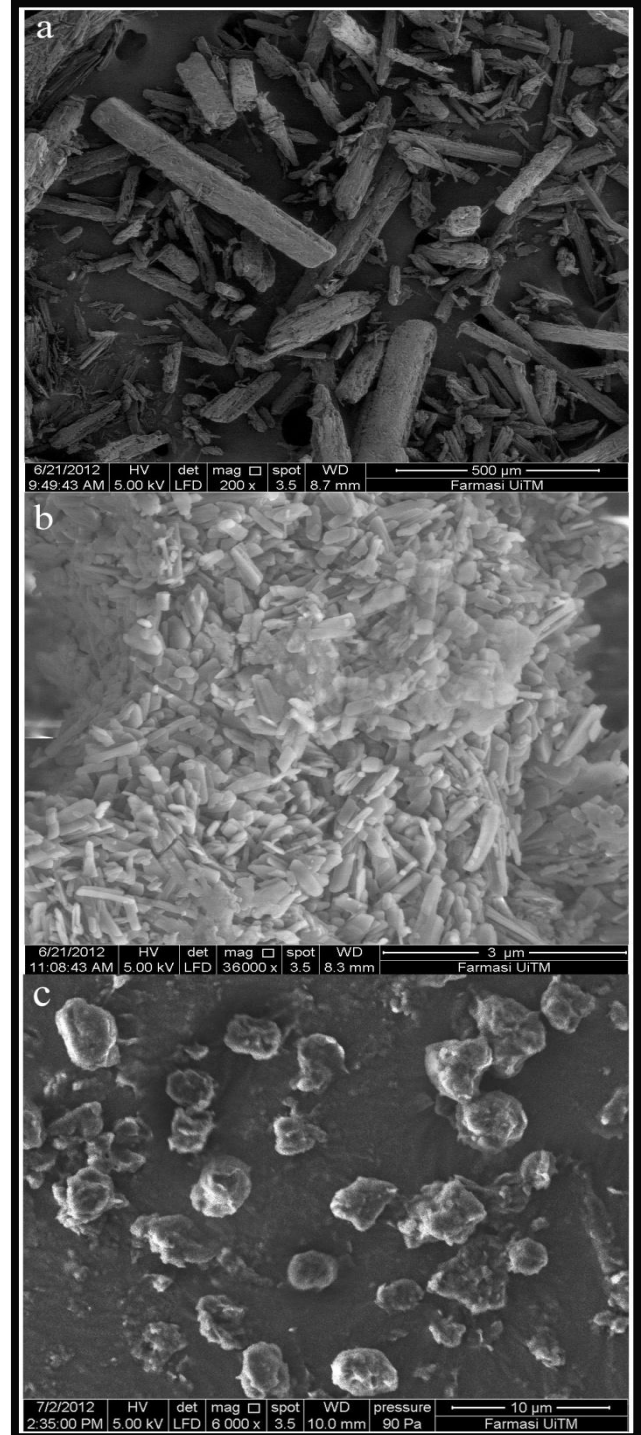


Figure 13: Scanning electron microscopy images of TP (a), TP – NPs (b) and F₀ (c)

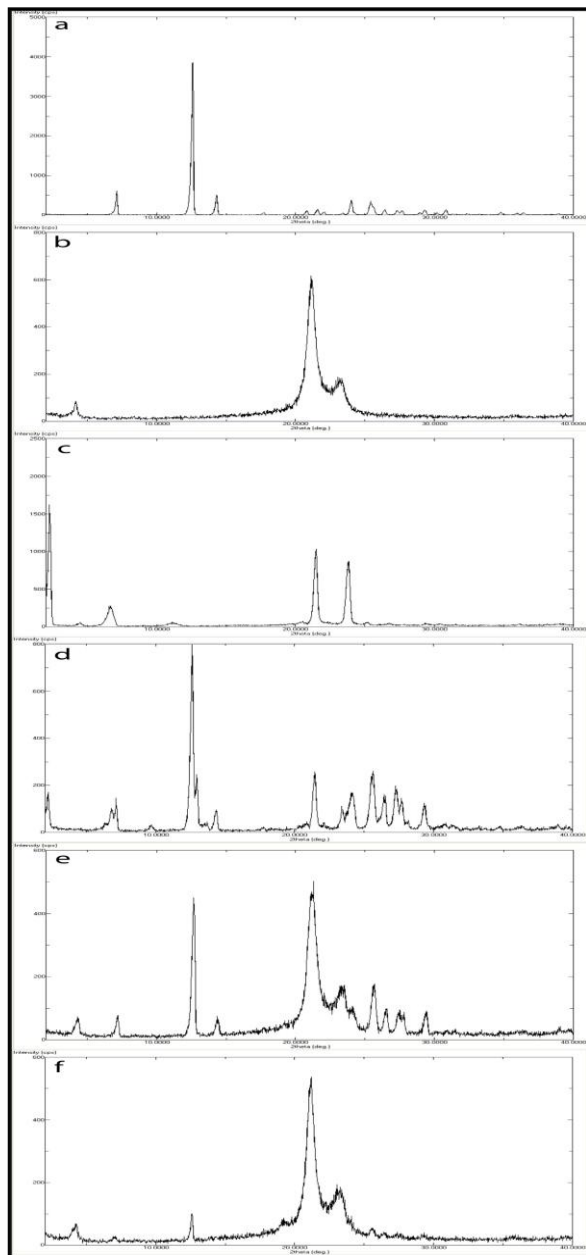


Figure 14: Powder X – ray diffraction Spectra of TP (a), GB (b), SA (c), TP – NPs (d), TP – GB physical mixture (e) and F₀ (f)

Conclusions

The selected variables main and interaction effects on the critical quality attributes of the inhalable solid lipid microparticles were determined by a Box – Behnken design of experiment. Theophylline level has a statistical influence over the entrapment efficiency, zeta potential and cumulative percentage released, whereas glyceryl behenate and poloxamer 188 have a significant effect on the mass median

aerodynamic diameter and fine particles fraction. Since theophylline is a narrow therapeutic index drug (10 – 20 µg / ml), i.e., very small dose locally can be efficient in nocturnal asthma and so each 10 mg of the optimized formula will hold approximately 500 µg of theophylline according to the software predicted values which are in a good correlation with the experimental values.

References

1. Marianecci C, Di Marzio L, Rinaldi F, Carafa M, Alhaique F. Pulmonary Delivery: Innovative Approaches and Perspectives. *Journal of Biomaterials and Nanobiotechnology* 2011; 2(5): 567 – 575.
2. Momeni A, Mohammadi MH. Respiratory Delivery of Theophylline by Size – Targeted Starch Microspheres for Treatment of Asthma. *Journal of Microencapsulation* 2009; 26(8): 701 – 710.
3. Frijlink HW, De Boer AH. Dry Powder Inhalers for Pulmonary Drug Delivery. *Expert Opinion in Drug Delivery* 2004; 1(1): 67 – 86.
4. Pritchard JN. The Influence of Lung Deposition on Clinical Response. *Journal of Aerosol Medicine* 2001; 14(S1): S19 – S26.
5. Adi S, Adi H, Tang P, Traini D, Chan H-K, Young PM. Micro – Particle Corrugation, Adhesion and Inhalation Aerosol Efficiency. *European Journal of Pharmaceutical Sciences* 2008; 35(1 – 2): 12 – 18.
6. Salama R, Traini D, Chan H-K, Young PM. Recent Advances in Controlled Release Pulmonary Therapy. *Current Drug Delivery* 2009; 6(4): 404 – 414.
7. Karathanasis E, Ayyagari AL, Bhavane R, Bellamkonda RV, Annapragada AV. Preparation of In Vivo Cleavable Agglomerated Liposomes Suitable for Modulated Pulmonary Drug Delivery. *Journal of Controlled Release* 2005; 103(1): 159 – 175.
8. Rytting E, Bur M, Cartier R, Bouyssou T, Wang X, Krüger M, Lehr C-M, Kissel T. In Vitro and In Vivo Performance of Biocompatible Negatively – Charged Salbutamol – Loaded Nanoparticles. *Journal of Controlled Release* 2010; 141(1): 101 – 107.
9. Sebti T, Amighi K. Preparation and In Vitro Evaluation of Lipidic Carriers and Fillers for Inhalation. *European Journal of Pharmaceutics and Biopharmaceutics* 2006; 63(1): 51 – 58.

10. Burioka N, Fukuoka Y, Koyanagi S, Miyata M, Takata M, Chikumi H, Takane H, Watanabe M, Endo M, Sako T, Suyama H, Ohdo S, Shimizu E. Asthma: Chronopharmacotherapy and the Molecular Clock. *Advanced Drug Delivery Reviews* 2010; 62(9 – 10): 946 – 955.
11. Mandal AS, Biswas N, Karim KM, Guha A, Chatterjee S, Behera M, Kuotsu K. Drug Delivery System Based on Chronobiology — A Review. *Journal of Controlled Release* 2010; 147(3): 314 – 325.
12. Ohdo S. Chronotherapeutic Strategy: Rhythm Monitoring, Manipulation and Disruption. *Advanced Drug Delivery Reviews* 2010; 62(9 – 10): 859 – 875.
13. Keravis T, Lugnier C. Cyclic Nucleotide Phosphodiesterase (PDE) Isozymes as Targets of the Intracellular Signalling Network: Benefits of PDE Inhibitors in Various Diseases and Perspectives for Future Therapeutic Developments. *British Journal of Pharmacology* 2012; 165(5): 1288 – 1305.
14. Lindenberg M, Kopp S, Dressman JB. Classification of Orally Administered Drugs on the World Health Organization Model List of Essential Medicines According to the Biopharmaceutics Classification System. *European Journal of Pharmaceutics and Biopharmaceutics* 2004; 58(2): 265 – 278.
15. Cook RO, Pannu RK, Kellaway IW. Novel Sustained Release Microspheres for Pulmonary Drug Delivery. *Journal of Controlled Release* 2005; 104(1): 79 – 90.
16. Box GEP, Behnken DW. Some New Three Level Designs for the Study of Quantitative Variables. *Technometrics* 1960; 2(4): 455 – 475.
17. Bei D, Marszalek J, Youan B-BC. Formulation of Dacarbazine – Loaded Cubosomes – Part I: Influence of Formulation Variables. *The American Association of Pharmaceutical Scientists PharmSciTech Journal* 2009; 10(3): 1032 – 1039.
18. Salem HF, Abdelrahim ME, Abo Eid K, Sharaf MA. Nanosized Rods Agglomerates as a New Approach for Formulation of a Dry Powder Inhaler. *International Journal of Nanomedicine* 2011; 6: 311 – 320.
19. He J, Hou S, Lu W, Zhu L, Feng J. Preparation, Pharmacokinetics and Body Distribution of Silymarin - Loaded Solid Lipid Nanoparticles After Oral Administration. *Journal of Biomedical Nanotechnology* 2007; 3(4): 195 – 202.
20. Fini A, Cavallari C, Ospitali F, Gonzalez-Rodriguez ML. Theophylline – Loaded Compritol Microspheres Prepared by Ultrasound – Assisted Atomization. *Journal of Pharmaceutical Sciences* 2011; 100(2): 743 – 757.
21. Bosquillon C, Lombry C, Pre´at V, Vanbever R. Comparison of Particle Sizing Techniques in the Case of Inhalation Dry Powders. *Journal of Pharmaceutical Sciences* 2001; 90(12): 2032 – 2041.
22. Abdelbary G, Fahmy RH. Diazepam – Loaded Solid Lipid Nanoparticles: Design and Characterization. *The American Association of Pharmaceutical Scientists PharmSciTech Journal* 2009; 10(1): 211 – 219.
23. Jaspert S, Bertholet P, Piel G, Dogne´ J-M, Delattre L, Evrard B. Solid Lipid Microparticles as a Sustained Release System for Pulmonary Drug Delivery. *European Journal of Pharmaceutics and Biopharmaceutics* 2007; 65(1): 47 – 56.
24. Sze A, Erickson D, Ren L, Li D. Zeta – Potential Measurement Using the Smoluchowski Equation and the Slope of the Current – Time Relationship in Electroosmotic Flow. *Journal of Colloid and Interface Science* 2003; 261(2): 402 – 410.
25. Padhi BK, Chougule MB, Misra A. Optimization of Formulation Components and Characterization of Large Respirable Powders Containing High Therapeutic Payload. *Pharmaceutical Development and Technology* 2006; 11(4): 465 – 475.
26. Salama RO, Traini D, Chan H-K, Young PM. Preparation and Characterization of Controlled Release Co – Spray Dried Drug – Polymer Microparticles for Inhalation. 2: Evaluation of In Vitro Release Profiling Methodologies for Controlled Release Respiratory Aerosols. *European Journal of Pharmaceutics and Biopharmaceutics* 2008, 70(1): 145 – 152.
27. Jensen LB, Magnusson E, Gunnarsson L, Vermehren C, Nielsen HM, Petersson K. Corticosteroid Solubility and Lipid Polarity Control Release From Solid Lipid Nanoparticles. *International Journal of Pharmaceutics* 2010, 390(1): 53 – 60.
28. Khan KA. The Concept of Dissolution Efficiency. *Journal of Pharmacy and Pharmacology* 1975; 27(1): 48 – 49.
29. May S, Jensen B, Wolkenhauer M, Schneider M, Lehr CM. Dissolution Techniques for In Vitro Testing of Dry Powders for Inhalation.

- Pharmaceutical Research 2012; 29(8): 2157 – 2166.
30. Solanki AB, Parikh JR, Parikh RH. Formulation and Optimization of Piroxicam Proniosomes by 3-Factor, 3-Level Box-Behnken Design. The American Association of Pharmaceutical Scientists PharmSciTech Journal 2007; 8(4): E1 – E7.
 31. Plumley C, Gorman EM, El – Gendy N, Bybee CR, Munson EJ, Berkland C. Nifedipine Nanoparticle Agglomeration as a Dry Powder Aerosol Formulation Strategy. International Journal of Pharmaceutics 2009; 369(1 – 2): 136 – 143.
 32. Muchow M, Maincent P, Müller RH. Lipid Nanoparticles with a Solid Matrix (SLN®, NLC®, LDC®) for Oral Drug Delivery. Drug Development and Industrial Pharmacy 2008; 34(12): 1394 – 1405.
 33. Obaidat AA, Obaidat RM. Controlled Release of Tramadol Hydrochloride from Matrices Prepared using Glyceryl Behenate. European Journal of Pharmaceutics and Biopharmaceutics 2001; 52(2): 231 – 235.
 34. Jelvehgari M, Barar J, Valizadeh H, Heidari N. Preparation and Evaluation of Poly (ϵ – Caprolactone) Nanoparticles – in – Microparticles by W / O / W Emulsion Method. Iranian Journal of Basic Medical Sciences 2010; 13(3): 85 – 96. <IVSL>
 35. Barreiro-Iglesias R, Bromberg L, Temchenko M, Hatton TA, Alvarez-Lorenzo C, Concheiro A. Pluronic – g – Poly (Acrylic Acid) Copolymers as Novel Excipients for Site Specific, Sustained Release Tablets. European Journal of Pharmaceutical Sciences 2005; 26(5): 374 – 385.
 36. Ekambaram P, Abdul HAS. Formulation and Evaluation of Solid Lipid Nanoparticles of Ramipril. Journal of Young Pharmacists 2011; 3(3): 216 – 220. <IVSL>
 37. Chow AHL, Tong HHY, Chattopadhyay P, Shekunov BY. Particle Engineering for Pulmonary Delivery. Pharmaceutical Research 2007; 24(3): 411 – 437.
 38. Katas H, Cevher E, Alpar HO. Preparation of Polyethyleneimine Incorporated Poly (D, L –Lactide – co – Glycolide) Nanoparticles by Spontaneous Emulsion Diffusion Method for Small Interfering RNA Delivery. International Journal of Pharmaceutics 2009; 369(1 – 2): 144 – 154.
 39. Abdelwahed W, Degobert G, Stainmesse S, Fessi H. Freeze – Drying of Nanoparticles: Formulation, Process and Storage Considerations. Advanced Drug Delivery Reviews 2006; 58(15): 1688 – 1713.
 40. Lu K, Kessler CS. Nanoparticle Colloidal Suspension Optimization and Freeze – Cast Forming. Synthesis and Processing of Nanostructured Materials 2007; 27(8): 1 – 10.
 41. Sinko PJ, Singh Yashveer. Martin’s Physical Pharmacy and Pharmaceutical Sciences 2011; 6th Edition: p. 384.
 42. Bihari P, Vippola M, Schultes S, Praetner M, Khandoga AG, Reichel CA, Coester C, Tuomi T, Rehberg M, Krombach F. Optimized Dispersion of Nanoparticles for Biological *in vitro* and *in vivo* Studies. Particle and Fibre Toxicology 2008; 5(1): 1 – 14.
 43. Nair AB, Goel A, Prakash S, Kumar A. Therapeutic Drug Monitoring By Reverse Iontophoresis. Journal of Basic and Clinical Pharmacology 2012; 3(1): 207 – 213. <IVSL>
 44. Viriyaraj A, Ritthidej GC. Diazepam – Glycerol Behenate Nanoparticles for Parenteral Delivery Prepared by the Hot Homogenization Process. Asian Journal of Pharmaceutical Sciences 2006; 1(1): 17 – 26.
 45. Vijayan V, Rao DS, Jayachandran E, Anburaj J. Preparation and Characterization of Anti Diabetic Drug Loaded Solid Lipid Microparticles. Journal of Innovative Trends in Pharmaceutical Sciences 2010; 1(8): 320 – 328. <IVSL>
 46. Martins S, Tho I, Ferreira DC, Souto EB, Brandl M. Physicochemical Properties of Lipid Nanoparticles: Effect of Lipid and Surfactant Composition. Drug Development and Industrial Pharmacy 2011; 37(7): 815 – 824.
 47. Shekunov PY, Chattopadhyay P, Tong HHY, Chow AHL. Particle Size Analysis in Pharmaceutics: Principles, Methods and Applications. Pharmaceutical Research 2006; 24(2): 203 – 227.
 48. Steckel H, Brandes HJ. A Novel Spray – Drying Technique to Produce Low Density Particles for Pulmonary Delivery. International Journal of Pharmaceutics 2004; 278(1): 187 – 195.
 49. Chougule MB, Padhi PK, Jinturkar KA, Misra A. Development of Dry Powder Inhalers. Recent Patents on Drug Delivery & Formulation 2007; 1(1): 11 – 21.
 50. Tantry JS, Tank J, Suryanarayanan R. Processing – Induced Phase Transitions of Theophylline: Implications on the Dissolution

- of Theophylline Tablets. *Journal of Pharmaceutical Science* 2007; 96(5): 1434 – 1444.
51. Üner M, Yener G. Importance of Solid Lipid Nanoparticles (SLN) in Various Administration Routes and Future Perspectives. *International Journal of Nanomedicine* 2007; 2(3): 289 – 300.
52. Abdul Qadir M, Rahman MS, Karim MZ, Akter S, Bin Awkat T, Reza MS. Evaluation of Hydrophobic Materials as Matrices for Controlled – Release Drug Delivery. *Pakistan Journal of Pharmaceutical Sciences* 2003; 16(2): 17 – 28.
53. Passerini N, Qi S, Albertini B, Grassi M, Rodriguez L, and Craig DQM. Solid Lipid Microparticles Produced by Spray Congealing: Influence of the Atomizer on Microparticle Characteristics and Mathematical Modeling of the Drug Release. *Journal of Pharmaceutical Sciences* 2010; 99(2): 916 – 931.
54. Gunasekaran S, Sankari G, Ponnusamy S. Vibrational Spectral Investigation on Xanthine and its Derivatives – Theophylline, Caffeine and Theobromine. *Spectrochimica Acta Part A: Molecular and Biomolecular Spectroscopy* 2005; 61(1 – 2): 117 – 127.
55. Brubach JB, Jannin V, Mahler B, Bourgaux C, Lessieur P, Roy P, Ovillon D. Structural and Thermal Characterization of Glyceryl Behenate by X – Ray Diffraction Coupled to Differential Calorimetry and Infrared Spectroscopy. *International Journal of Pharmaceutics* 2007; 336(2): 248 – 256.
56. Mezzena M, Scalia S, Young PM, Traini D. Solid Lipid Budesonide Microparticles for Controlled Release Inhalation Therapy. *The American Association of Pharmaceutical Scientists Journal* 2009; 11(4): 771 – 777.